

Global response of Martian plasma environment to an interplanetary structure: From ENA and plasma observations at Mars

Y. Futaana^{a,b}, S. Barabash^b, A. Grigoriev^b, D. Winningham^c, R. Frahm^c,
M. Yamauchi^b, and R. Lundin^b

^a Institute of Space and Astronautical Science, Japan Aerospace Exploration
Agency, Yoshinodai 3-1-1, Sagami-hara, 229-8502 Kanagawa, Japan

^b Swedish Institute of Space Physics, Box 812, SE-981 28 Kiruna, Sweden

^c Southwest Research Institute, San Antonio, TX 7228-0510, USA

Manuscript Pages: 28

Figures: 8

Tables: 0

Manuscript Revision: 1670

Abstract

As a part of the global plasma environment study of Mars and its response to the solar wind, we have analyzed a peculiar case of the subsolar energetic neutral atom (ENA) jet observed on June 7, 2004 by the Neutral Particle Detector (NPD) on board the Mars Express satellite. The “subsolar ENA jet” is generated by the interaction between the solar wind and the Martian exosphere, and is one of the most intense sources of ENA flux observed in the vicinity of Mars. On June 7, 2004 (orbit 485 of Mars Express), the NPD observed a very intense subsolar ENA jet, which then abruptly decreased within ~ 10 sec followed by quasi-periodic (~ 1 min) flux variations. Simultaneously, the plasma sensors detected a solar wind structure, which was most likely an interplanetary shock surface. The abrupt decrease of the ENA flux and the quasi-periodic flux variations can be understood in the framework of the global response of the Martian plasma obstacle to the interplanetary shock. The generation region of the subsolar ENA jet was pushed towards the planet by the interplanetary shock; and therefore, Mars Express went out of the ENA jet region. Associated global vibrations of the Martian plasma obstacle may have been the cause of the quasi-periodic flux variations of the ENA flux at the spacecraft location.

1 Introduction

The Martian plasma environment has been explored since the 1960s by the Mariner 4, and Mars 2, 3 and 5 spacecraft (e.g. see review by *Vaisberg* (1992)). Phobos 2 (1989) was the first mission to carry a complete set of modern

plasma experiments (e.g. *Sagdeev and Zakharov* (1989) and other articles in the Phobos-2 special issue [*Nature*, 341, pp 581-618, 1989]). In 1998, the Mars Global Surveyor (MGS) spacecraft carried a magnetometer and an electron reflectometer (MAG/ER) to investigate the magnetic properties of Mars (e.g. see review by *Nagy et al.* (2004)). In 2003, the Mars Express spacecraft arrived at Mars. The Analyser of Space Plasma and Energetic Atoms (ASPERA-3) on board Mars Express is the first comprehensive plasma and neutral particle package capable of measuring ions, electrons and energetic neutral atoms (ENAs) to explore the vicinity of Mars [*Barabash et al.* (2004)].

Mars has no global intrinsic magnetic field, but locally magnetized areas distributed globally. The MGS MAG/ER found strong magnetic fields of crustal origin, especially in the southern hemisphere [*Acuña et al.* (1998); *Acuña et al.* (1999)]. Owing to the lack of the global magnetic field and the existence of the strong and localized magnetic field, the interaction of Mars with the solar wind is much different than that of the Earth.

Our knowledge of the global Martian plasma environment is an average view. Temporal changes of the global Martian plasma environment are not well understood, particularly over short time scales. It is generally difficult to investigate temporal variations of global structure from *in situ* observations by a single spacecraft. One way to investigate the global Martian plasma environment from a single spacecraft is to analyze accumulated data statistically. For example, *Vignes et al.* (2002) used 553 bow shock crossings to investigate boundary locations from MGS MAG/ER data relative to solar wind conditions.

Energetic Neutral Atom (ENA) imaging techniques have developed rapidly

during the last decade. ENA imaging has become a powerful means to remotely investigate the plasma environment and the neutral exosphere of planets. Several Earth-orbiting spacecraft have carried ENA imagers to investigate the dynamics of the terrestrial plasma environment, such as in the auroral ionosphere, the cusp, the radiation belt, and the plasmashet (e.g. *Roelof et al. (1985)*; *Barabash et al. (1998)*; *Mitchell et al. (2000)*; *Pollock et al. (2000)*; *Moore et al. (2000)*).

Although ENA generation in the vicinity of Mars is quite different from that of the Earth (*Barabash et al. (2004)* and references therein), ENA imaging is still a powerful tool in order to investigate the spatial structures and temporal variations of the global plasma environment of Mars. Understanding of the Martian ENA environment is one of the main scientific goals for the ASPERA-3 experiment. The ASPERA-3 comprises four instruments: two ENA sensors, an electron spectrometer and an ion mass analyzer [*Barabash et al. (2004)*]. The two ENA sensors are called the Neutral Particle Imager (NPI) and the Neutral Particle Detector (NPD). Note that Mars Express does not carry a magnetometer. The initial results of ENA imaging have, in general, confirmed theoretical predictions as summarized below.

Kallio and Barabash (2001) has calculated the flux of ENAs emitted from the dayside Martian exobase. In their calculations, the solar wind ENAs (charge-exchanged solar wind protons in the upstream region of the bow shock) can reach very low altitudes within the Martian atmosphere, where elastic and inelastic collisions become dominant. As a result, some of the solar wind ENAs are expected to be scattered back into the space. *Futaana et al. (2006a)* confirmed the existence of such backscattered ENAs from the Martian upper atmosphere by analyzing the NPD data. The backscattered ENAs are emitted

globally with the flux of $\sim 10^7 \text{cm}^{-2}\text{s}^{-1}$. The observed signatures are consistent with calculations, while the only difference was that the flux of the backscattered ENAs was higher than in theoretical calculations. They concluded that the flux of the backscattered ENAs which originated from the direct input of the solar wind protons is significant at Mars.

Kallio et al. (2006) suggested an “ENA occultation” technique: part of the so-called solar wind ENAs, which are produced by charge exchange between solar wind protons and extended exosphere, are expected to be scattered in the near-Mars exosphere around the planetary limb, penetrating into the Martian tail. The ENA occultation is similar to stellar, solar wind and radio occultation measurements. In this ENA occultation technique, the ENAs penetrating into the tail region are used to infer information about the Martian exosphere. *Kallio et al.* (2006) also simulated the solar wind ENAs penetrating into the Martian tail as a separate ENA population. They used a Monte-Carlo model to simulate the interaction of these ENAs with the Martian atmosphere. Although their simulation predicted that the ENA flux was too low to be observed by existing instruments, it is worthwhile examining whether these ENAs are detectable by ASPERA-3. *Brinkfeldt et al.* (2006) reported on NPI analysis of signals from the direction around the limb during transversals of the Martian optical umbra. By comparing with simulations, they concluded that the NPI signals can also be explained by a ~ 20 eV perpendicular temperature of the solar wind protons. However at present, there are no reference observations of the solar wind temperature, and the above discussion still remains an open question.

Mars Express also found a substantial flux of ENAs in the direction tangential to the solar wind flow direction. *Gunell et al.* (2006) reported ENA signals

coming from the dayside magnetosheath observed by NPI. By comparing NPI data with an ENA generation model in the shocked solar wind [*Kallio et al. (1997)*], they concluded that these observations are ENAs of shocked solar wind origin. On the other hand, *Futaana et al. (2006b)* showed ENA emission from the subsolar region detected by the NPD instrument. The flux is denoted as a subsolar ENA jet (or cone) because the emitted flux is highly directional from the subsolar region. The question whether these ENA observations by different instruments are of the same origin is still under investigation.

As discussed in *Futaana et al. (2006b)*, we can consider two possible source for the subsolar ENA jet: shocked solar wind protons and protons of planetary origin. The first source was discussed by *Holmström et al. (2002)*, and is responsible for the ENA flux detected by NPI (*Gunell et al. (2006)*). When the shocked solar wind protons charge exchange with exospheric particles, they are converted to ENAs and form the subsolar ENA jet. The second source is described in *Lichtenegger et al. (2002)*. After photoionization of the exospheric cold neutral atoms, the resulting ions are accelerated via energy or momentum exchange [*Peréz-de-Tejada (1987)*] with the shocked solar wind, eventually reaching the same energy or momentum as the shocked solar wind. When such accelerated ions experience the charge exchange reaction, they are observed as a subsolar ENA jet.

No matter what the subsolar ENA jet generation mechanism is, we can conclude that the jet is generated in the vicinity of the subsolar region of the Martian upper atmosphere as a result of the interaction between the solar wind and the Martian upper atmosphere. This means that detailed investigations of subsolar ENA jets would advance the understanding of the dynamics involved in the interaction between the planet and the solar wind.

In this paper, we analyze a peculiar subsolar ENA jet event which was recorded by the NPD on June 7, 2004 (orbit 485) and discuss the global Martian plasma environment. For this event, the NPD measured an extremely high flux of ENAs from a subsolar ENA jet. This strong ENA flux decreased abruptly over a time scale of ~ 10 sec. Following the decrease, periodic enhancements of ENA fluxes were observed. We show the NPD data together with *in situ* plasma data to investigate global signatures of the interaction between the Martian upper atmosphere and the solar wind.

2 Instrumentation and Data

2.1 Neutral Particle Detector

The Mars Express spacecraft carried the first ENA instrument to Mars as a part of the Analyser of Space Plasma and Energetic Atoms (ASPERA-3) experiment [Barabash *et al.* (2004)]. The ENA instrument is composed of two sensors: the Neutral Particle Imager (NPI) and the Neutral Particle Detector (NPD). The NPI is designed to measure ENAs with high angular resolution ($\sim 4.5^\circ \times 11.25^\circ$) and with a total field of view of 360° (32 directions), but without mass and energy resolution. The NPD can resolve particle velocities and masses, but possesses a lower angular resolution ($\sim 5^\circ \times 40^\circ$) and only has total field view of $\sim 180^\circ$ (6 directions). For the analysis in this paper, we used only NPD data as a measure of the ENA flux.

The NPD sensor consists of two identical detectors, NPD-1 and NPD-2, each containing three directions (Dirs-0, -1 and -2) that form approximately a 90° fan. We used only two directions of NPD-1 during this analysis. The NPD

measures ENA differential flux over the energy range 100 eV-10 keV, resolving H and O. The velocity is obtained by measuring the time-of-flight (TOF) of each ENA [Barabash *et al.* (2004)]. The nominal operation mode of the NPD is the ‘bin-matrix’ mode. In this mode, each TOF signal is accumulated into 16 logarithmically-divided TOF bins (50-1900 nsec). In order to analyze TOF spectra of ENAs, the recorded count rate in each TOF bin [counts/sec] is normalized by dividing by the TOF window width [nsec]. The time resolution for ENA detection is 1 sec [Futaana *et al.* (2006b)].

Since the NPD is an open system, there exist background counts due to ultraviolet (UV) photons which enter into the detector. UV photons can stochastically generate correlated signals, which are not ENA-originated signals. This background level is not constant, but has temporal changes due to the change in the local UV flux, i.e. from the spacecraft location and the direction of instrument aperture. We have regarded the correlated counts recorded in the TOF channel of 1514-1900 ns (corresponding to 14-22 eV/amu) as the background level. Since the MCP response to ENAs is extremely low in this energy range (~ 20 eV), all of this channel’s counts are considered as UV-originated counts. Theoretically, the background level has a TOF dependence, but the difference is not large (less than 10%) in the TOF range of the NPD. Therefore, we have assumed a constant background level over the TOF range. The background level has been subtracted from the TOF data before analyses.

2.2 Plasma Spectrometers

The ASPERA-3 observes *in situ* plasma velocity distribution functions by using two plasma sensors: the Electron Spectrometer (ELS) and the Ion Mass

Analyzer (IMA) [*Barabash et al. (2004)*]. The ELS is a spherical top-hat analyzer with the aperture of $4^\circ \times 360^\circ$. There are 16 anodes corresponding to the directions of the incident electrons, and each has an angular resolution of $\sim 4^\circ \times 22.5^\circ$. The ELS provides two-dimensional electron velocity distribution functions over the energy range of ~ 0.4 eV-20 keV with 128 energy steps. The time resolution (i.e. the time for one energy sweep of the top-hat analyzer) is 4 sec.

The IMA can perform quasi-three-dimensional ion observations within the energy range of ~ 10 eV-30 keV in 96 energy steps. The total field of view is $90^\circ \times 360^\circ$ with an angular resolution of $\sim 5.6^\circ \times 22.5^\circ$. The IMA possesses an electrostatic deflection system (elevation analyzer) in front of a top-hat analyzer to obtain 3-D ion velocity distribution functions. By sweeping the voltage of the deflector, the view angle can be changed by $\pm 45^\circ$ with respect to the aperture plane of the top-hat analyzer. Each energy sweep takes 12 sec, and a 3-D distribution function is obtained by completing an angular sweep with the time resolution of 192 sec.

3 Observations

Figure 1 shows the Mars Express orbit in the cylindrical Mars-Sun orbit (MSO) coordinate system from 11:00 to 14:30 UT on June 7, 2004 (orbit 485). The pericenter was at 13:22:26 UT with an altitude of ~ 260 km from the Martian surface. In this figure, the dotted lines show the average locations of the modeled bow shock (BS) and the magnetic pileup-boundary (MPB) determined by *Vignes et al. (2000)*. The bow shock is the region created in front of the Martian plasma obstacle where the solar wind is decelerated from super-

sonic to subsonic speed. The MPB is the boundary where the magnetic field becomes strong and the electron flux is decreased (e.g. *Nagy et al. (2004)*). These models were derived from statistical studies from Mars Global Surveyor (MGS) observations, but it is known that these boundaries are highly variable depending on upstream conditions. Therefore, we need to identify these boundaries using the *in situ* plasma data for analysis of this single event.

Figure 1

Figure 2 shows the plasma observations between 11:00 and 14:15 UT. From top to bottom, the energy-time spectra for ELS (CH-3 and -7) and IMA are displayed. The periodic change (~ 3 min) within the IMA data is due to the angular sweep of the electrostatic deflection system (see Section 2).

Figure 2

Mars Express was in the upstream solar wind region when the plasma observations started ($\sim 11:15$ UT), and approached Mars from its nightside. At $\sim 12:07$ UT, Mars Express crossed the bow shock as indicated by sharp increase of the electron and the ion temperatures. The crossing position is drawn by the filled symbol (BS_{in}) in Figure 1, which shows that the bow shock was located much closer to Mars than predicted by the model. The ion count gradually decreased between 12:53-13:02 UT. These changes in solar wind ions were due to the crossing of the stopping boundary of the solar wind. *Lundin et al. (2004)* named this solar wind stopping boundary the induced-magnetosphere boundary (IMB). Because the IMB has a finite thickness in general, we used two definitions of the IMB: the topside IMB (IMB_T) and the bottomsides IMB (IMB_B). The IMB_T is the boundary where the shocked solar wind flux and velocity start to decrease (12:53 UT, IMB_{Tin}), and the IMB_B is the boundary

where shocked solar wind disappears (13:02 UT, IMB_{Bin}). Note that Mars Express was in the umbra region between 12:58-13:20 UT. The outbound IMB_B and IMB_T crossings are identified as 13:31 (IMB_{Bout}) and 13:36 UT (IMB_{Tout}), respectively. At around 13:47 UT, Mars Express crossed the bow shock (BS_{out}) again and exited to the solar wind region. One can also see a change of the solar wind conditions at around 13:58:30 UT.

The bow shock and the IMB shape and location during the observation can be fitted by the boundary crossing positions identified above. Here we applied the scaling law to the boundary location models by *Vignes et al.* (2000), which are the average locations of the bow shock and the MPB calculated by 290 orbits of Mars Global Surveyor. For fitting the bow shock shape, we used the positions of inbound (BS_{in}) and outbound (BS_{out}) bow shock crossing. For fitting the IMB shape, we used the outbound IMB crossing positions (IMB_{Bout} and IMB_{Tout}) under the assumption that the IMB and the MPB are identical. The fitted boundaries are shown by dashed lines in Figure 1. The scaling factors are ~ 0.77 and ~ 0.90 for the bow shock and the IMB, respectively. We can conclude that during orbit 485, the dayside Martian plasma environment was substantially compressed compared to its average size.

Figure 3 shows MGS dynamic pressure proxy data between 0:00-18:00 UT on June 7 at Mars. The magnetic field data observed by MGS were converted to the solar wind dynamic pressure by assuming pressure balance. The time resolution of the data is 2 hours (corresponding to the MGS orbital period), and each estimate has been generated by fitting the magnetic field data from the dayside northern hemisphere (~ 30 min) [*Cridder et al.* (2003)]. The dynamic pressure (P_{dy}) was a typical value of ~ 0.5 nPa before 6:00 UT. Figure 3 also shows that there are two increases of P_{dy} : at 8:00 UT to ~ 2.5 nPa and at

14:00 UT to ~ 6 nPa. This solar wind pressure is extremely large in the vicinity of Mars.

Figure 3

The NPD-1 observation during this orbit is shown in Figure 4(a) and (b). The instrument was on between 13:42 and 14:13 UT on June 7, 2004. The vertical axis is the TOF of the ENAs, which is converted to the hydrogen ENA energy as shown on the right axis. The background levels have been subtracted from the observed TOF spectra as described in Section 2. Only directions 1 and 2 (Dirs-1 and -2) observe the ENA jet flow. Figure 4(c) shows the instrument count rate integrated over the range 50-1900 ns (corresponding to 14 eV-20 keV). The maximum count rate was ~ 1000 counts/s, which corresponds to a flux of $J = (0.6-1) \times 10^7 \text{ cm}^{-2} \text{ sr}^{-1} \text{ s}^{-1}$, where we employ the geometric factor (G_0) and efficiency (ϵ) of $\epsilon \cdot G_0 = (9.78-17.1) \times 10^{-5} \text{ cm}^2 \text{ sr}$ for 1 keV hydrogen atoms. This flux is approximately 5 times higher than the typical flux of $(1-2) \times 10^6 \text{ cm}^{-2} \text{ sr}^{-1} \text{ s}^{-1}$ [Futaana et al. (2006b)]. The observed energy of this ENA jet (0.8-3.0 keV corresponding to $\sim 390-760$ km/s for hydrogen ENAs) is consistent with the typical subsolar ENA jet.

Figure 4

Figure 5 shows a fish-eye projection of geometry of Mars with respect to the field of view (FOV) of the NPD. The dark and light gray rectangles correspond to the Dirs-1 and -2 FOVs, respectively. Mars and the fitted IMB are shown by the black and the gray curves. The Mars-sun line is also indicated by a black hair line with filled symbols at 0, 500, 1000 and 3397 km above the subsolar point. The observation geometry, the intensity, and the energy of the ENAs suggest that the intense ENA signal before 13:58:40 UT comes from

the subsolar region, which is the subsolar ENA jet reported by *Futaana et al.* (2006b).

Figure 5

A notable signature in this observation is the abrupt decrease of the subsolar-ENA flux at 13:58:40 UT within ~ 10 sec, i.e. a distance of 30 km. Moreover, after the ENA flux has decreased, the NPD observed quasi-periodic enhancements with three peaks in the ENA flux (indicated by three arrows in Figure 4(c)) up to 200 counts/sec (which is the typical count rate of subsolar ENA jets) . The time interval between each peak is ~ 1 min.

4 Discussion

As described in the introduction, the subsolar ENA jet is a result of the interaction between the solar wind and the Martian upper atmosphere. Stationary characteristics of the observed subsolar ENA jet were investigated by *Futaana et al.* (2006b). In 38 orbits with favorable FOV configurations of the NPD, the subsolar ENA jet can be detected in 36 orbits. Moreover, one third of the outer boundaries of the subsolar ENA jets exhibit clear edges. The typical time scale for the crossing this boundary is about 1 min, which corresponds to a thickness of 200 km for the outer boundary.

However, the ENA jet observed during the orbit 485 shows three peculiarities: the flux is ~ 5 times higher than the nominal jet flux, the outer boundary is extremely clear (corresponding to the abrupt decrease within ~ 10 sec at $\sim 13:58:40$ UT), and there are quasi-periodic enhancements (~ 1 min) just after the boundary crossing. Since these characteristics are quite unique, it is

difficult to interpret them by using nominal solar wind modulations.

One possible interpretation is that the change is caused by crustal magnetized regions of Mars [Acuña *et al.* (1998); Acuña *et al.* (1999)]. A magnetic anomaly can reconfigure the MPB shape and the location of the subsolar region [Cridder *et al.* (2002)], and the change in the MPB may explain the peculiarities. However, this idea is not feasible because the subsolar point at the time of the observations was $\sim(45^\circ\text{E}, 17^\circ\text{N})$, where crustal magnetization is very weak. It is also difficult to reconfigure the MPB within the time scale of 10 sec (corresponding to the 0.04° rotation of Mars).

Another idea is that these signatures are caused by temporal variations in the Martian plasma environment triggered by an change in the solar wind dynamic pressure. This idea well explains these signatures, and is consistent with simultaneous plasma observations.

The first peculiarity of the extremely high ENA flux observed before the abrupt decrease can be interpreted as the result of a compressed Martian plasma obstacle. The bow shock and the IMB were closer to Mars than the average locations of these boundaries, as described in the previous section. This means that the Martian plasma obstacle was more compressed and smaller than the average (Figure 1). This compression might be a result of the increase in solar wind dynamic pressure at 8:00 UT (Figure 3). Under a compressed configuration, the magnetosheath solar wind ions can reach lower altitudes, where the neutral particle density is higher. The scale height at the height of the exobase is about 30 km [Fox and Dalgarno (1979)]. So therefore, the intensity of the ENA jet is expected to be sensitive to the compression of the IMB. Assuming exponentially decreasing exosphere with height, 5 times

higher density corresponds to a decrease of 48 km in altitude, which is not an unreasonable value.

The second peculiarity, the abrupt decrease in ENA flux at $\sim 13:58:40$ UT, is interpreted as a result of a clear solar wind structure crossing as indicated by the ion and the electron observations ($13:58:30$ UT). This structure may be correlated with the second increase in the dynamic pressure which occurred sometime between $\sim 13:30$ and $14:00$ (Figure 3).

Figure 6 shows detailed plots of the simultaneous plasma observations obtained by the ELS and the IMA after the bow shock crossing ($13:47$ UT). From top to bottom, (a) flux of the NPD, (b) the energy-time (E-t) spectrogram for the ELS, (c) the time series of the electron count rate for 5 energy ranges, (d) the E-t spectrogram for the IMA, (e) the energy mass spectrograms for the IMA are displayed. Figure 6(e-1) and (e-2) display the energy-mass spectra integrated over all the viewing direction of IMA before and after the solar wind conditions changed at $\sim 13:58:30$ UT. The thick lines show the mass per charge (M/q) profiles for selected mass species.

Figure 6

The bow shock crossing was at $\sim 13:47$ UT, and afterward Mars Express was in the solar wind. By using the electron data, it can easily be identified that the solar wind conditions changed at $\sim 13:58:30$ UT (indicated by arrows). Features are also observed in the electron flux enhancements ($< 20\text{eV}$) between $13:59$ - $14:04$ UT; however these flux enhancements are an artifact signatures, which may be due to photoelectrons of satellite or instrument origin. These fluxes are always observed when special viewing configurations occur. The change in the solar wind at $\sim 13:58:30$ UT is not the artifact; the undisturbed

electron fluxes at 13:50-13:55 and 14:05-14:10 are clearly changed. Such a change in spectra is not observed in data from other orbits.

Lacking magnetic field data, it is difficult to tell whether this abrupt flux change is caused by a shock or a discontinuity. However, there are several characteristics of the plasma observations which strongly suggesting that this solar wind structure was indeed an interplanetary shock. First, the electron flux with energies larger than 150 eV was increased while the flux with energies less than 50 eV was decreased (Figure 6 (b) and (c)). This signature can be interpreted as the superthermal electron heating by an interplanetary shock [e.g. *Feldman et al. (1983); Treumann and Terasawa (2001)*]. Simultaneously, IMA data in Figure 6(d) indicate that the solar wind ions were heated and the velocity distribution function was broadened. We also see nonthermal ions with an energy range of 2-10 keV around the time of the solar wind structure crossing (\sim 13:59 UT). The energy-mass spectrum (Figure 6(e-2)) indicates that the ions are protons ($M/q=1$). Since we cannot see such nonthermal protons before the solar wind structure crossing (Figure 6(e-1)), these nonthermal protons are generated by the solar wind structure. We can conclude that the nonthermal ions are solar wind protons reflected at the supercritical shock surface [e.g. *Thomsen (1985)*] since such nonthermal ions are observed as well in the vicinity of shock surfaces. Moreover, such reflected ions do not theoretically exist in the vicinity of discontinuities. From the above investigations, the solar wind structure is most likely an interplanetary shock.

The explanation of how the interplanetary shock surface (even if the interface is not the shock, but just the increase of the dynamic pressure) results in the abrupt decrease of the ENA jet flux is illustrated in Figure 7. As shown in Figure 7(a), Mars Express was in the ENA jet. After the interplanetary shock

surface hit the Martian plasma obstacle, the obstacle was compressed due to the higher dynamic pressure of the downstream medium of the interplanetary shock (Figure 7(b)). This is analogous to the sudden commencement at the Earth’s magnetosphere [e.g. *Araki (1994)*]. Under the compressed situation, the obstacle moved closer to Mars and the solar wind streamlines changed. The reconfiguration of the obstacle shape and location caused the ENA jet generation region to move closer to the planet. The reconfiguration also change the shape of the generation region. As a result, the satellite exited from the jet region. Even though the FOV looked toward the generation region, the plasma streamlines at the subsolar region did not point toward the satellite. As a result, no flux could not be detected.

Figure 7

The third peculiarity of this observation is the quasi-periodic enhancements of ENA flux occurring just after the abrupt decrease. The period is ~ 1 min and we observed at least three peaks in the data (13:59-14:05 UT, arrows in Figure 4(c)). The generation mechanism of these enhancement is still an open question, but one possible candidate is that there were global vibrations of the Martian plasma obstacle triggered by the interplanetary shock. Such global vibrations cause the jet generation region to move back and forth resulting in variations of the ENA flux at the satellite location. From *in situ* observations conducted by the Phobos 2 and Mars Global Surveyor spacecraft, ultra low-frequency magnetic oscillations in the Martian magnetosheath have been observed while the mechanism that causes such the oscillations is not yet known [*Espley et al. (2004)*]. This kind of global vibration of the plasma obstacle can provide one possible explanation for the quasi-periodic enhancement in jet flux just after its abrupt decrease, but careful investigations by

global hybrid simulations are necessary and are yet to be performed.

We should note that it is possible for the global structure of the ENA jet to be influenced by the interaction with an inclined interplanetary shock. If the interplanetary shock had an inclination (defined by the angle between the Mars-Sun line and the normal direction of the interplanetary shock), the interplanetary shock would hit the flank-side of the Martian plasma obstacle. This may introduce an observable reconfiguration of the ENA jet as well, which in turn could result in the decrease of the ENA jet flux at the satellite location.

However, the simple calculation below shows that the interplanetary shock was nearly perpendicular to the Mars-Sun line during this event. Figure 8 shows the 7-min observation of the ELS flux and the NPD count rate around the interplanetary shock crossing. The time of the shock arrival of the satellite position is $\sim 13:58:30$ UT as determined from the ELS observation (Figure 8(a)), while the ENA decrease starts at $\sim 13:58:40$ UT (Figure 8(b)). The distance between the Martian subsolar region and Mars Express was $L \sim 4400$ km (see Fig. 1). The ENAs (average velocity was $v \sim 575$ km/s) took $T \sim 7.7$ sec to arrive at the spacecraft location after their generation in the subsolar region. This means that the interplanetary shock hit the Martian plasma obstacle at around $13:58:32$ UT, which was approximately the same time as when the shock was detected by Mars Express. Since the x -coordinate of Mars Express at the interplanetary shock crossing was almost the same as that of the Martian magnetic obstacle as seen in Fig. 1, we conclude that the interplanetary shock could have a small inclination.

Figure 8

From this peculiar event, we are also able to discuss the extent of the subsolar jet generation region by the investigation of the travel time for the ENAs which forms the jet. The extent of the generation region along the line of sight, ΔL , can be estimated by the decrease time of the ENA jet flux at the satellite position, ΔT , and the dispersion of the ENA velocity. The relationship is described as

$$\left(\frac{\Delta L}{L}\right)^2 \sim \left(\frac{\Delta T}{T}\right)^2 + \left(\frac{\Delta v}{v}\right)^2,$$

where T and L is the average travel time and the distance between the generation region and the satellite, v is the velocity of the ENA, and Δv is the deviation of the ENA velocity. Figure 8(b) shows that it took $\Delta T \sim 10$ sec for the ENA flux decrease (13:58:40-13:58:50 UT). T and L are about 7.7 sec and 4400 km from the above discussion. The observed ENA energies are 800 eV-3 keV (Figure 4), which corresponds to the hydrogen ENA velocities of 390-760 km/s, i.e., $v \sim 575$ km/s and $\Delta v \sim 370$ km/s. Using these values, the extent ΔL is calculated as 6400 km. This extent is approximately the same order as the Martian diameter.

5 Summary

The NPD data obtained on June 7, 2004 (orbit 485) exhibited an extremely high flux of a subsolar ENA jet. The observed flux was approximately 5 times higher than the typical ENA jet flux, and abruptly decreased over a very short time (less than 10 sec), when the spacecraft crossed the outer boundary of the ENA jet. We interpret this peculiar event as a result of a quick reconfiguration of the Martian plasma environment due to the arrival of a solar wind structure.

A simultaneous structure showing a pressure increase was also observed in the MGS dynamic pressure data. The simultaneous *in situ* ion and electron observations showed a clear boundary in the solar wind at the time of the decrease of the ENA jet. The solar wind ions and electrons were heated after the solar wind boundary crossing and generation of the reflected ions was observed. Because these signatures are commonly observed in the vicinity of shock surfaces, the change in the interplanetary medium was most likely due to an interplanetary shock.

When the interplanetary structure hit the Martian plasma obstacle, the IMB was pushed toward the planet and the generation region of the subsolar ENA jet moved toward Mars (Figure 7). This global reconfiguration could cause the sudden decrease of the subsolar ENA jet observed at the Mars Express location. After the sudden decrease, the ENA flux exhibited quasi-periodic enhancements with a period of ~ 1 min. This periodic flux may be interpreted as a result of the global vibration of the Martian plasma obstacle with a characteristic frequency of ~ 1 min.

This NPD observation provided information about the response in the Martian plasma environment to a change in solar wind conditions. The Martian plasma obstacle responds to the solar wind change on a very short time scale (~ 10 sec). Moreover, the response appears to be elastic, and a solar wind dynamic pressure pulse can induce a global vibration mode of the Martian plasma environment with ~ 1 min period.

The event reported in this paper is unique. When the interplanetary shock reached the Martian plasma obstacle, the spacecraft was located in the ENA jet, and we have plasma and neutral particle data during this event. Unfortu-

nately, no statistical analysis is possible at present.

We would like to emphasize that the observations of subsolar ENA jets can be used as a global monitoring tool to investigate the dynamics of the Martian plasma obstacle. Such a remote observation of the plasma environment is one advantage of ENA imaging. By comparing *in situ* plasma observations and remote ENA observations, one can investigate global signatures of the interaction between the Martian upper atmosphere and the solar wind.

References

- Acuña, M. H., J. E. P. Connerney, P. Wasilewski, R. P. Lin, K. A. Anderson, C. W. Carlson, J. McFadden, D. W. Curtis, D. Mitchell, H. Rème, C. Mazelle, J. A. Sauvaud, C. d’Uston, A. Cros, J. L. Medale, S. J. Bauer, P. Cloutier, M. Mayhew, D. Winterhalter, and N. F. Ness, 1998. Magnetic field and plasma observations at Mars: Initial results of the Mars Global Surveyor mission, *Science*, *279*, 1676–1680.
- Acuña, M. H., J. E. P. Connerney, N. F. Ness, R. P. Lin, D. Mitchell, C. W. Carlson, J. McFadden, K. A. Anderson, H. Rème, C. Mazelle, D. Vignes, P. Wasilewski, and P. Cloutier, 1999. Global distribution of crustal magnetization discovered by the Mars Global Surveyor MAG/ER experiment, *Science*, *284*, 790–793.
- Araki, T., 1994. A physical model of the geomagnetic sudden commencement, in *Solar Wind Sources of Magnetospheric Ultra-Low-Frequency Waves*, *Geophysical Monograph*, vol. 81, edited by M. J. Engebretson, K. Takahashi, and M. Scholer, pp. 183–200.
- Barabash, S., O. Norberg, R. Lundin, S. Olsen, K. Lundin, P. C. Brandt, E. C.

- Roelof, C. J. Chase, B. H. Mauk, H. Koskinen, and J. Rynö, 1998. Energetic neutral atom imager on the Swedish microsatellite Astrid, in *Measurement techniques in space plasmas, Field*, edited by R. F. Pfaff, J. E. Borovsky, and D. T. Young, AGU Geophysical Monograph 103, pp. 257–262, American Geophysical Union, Washington, DC.
- Barabash, S., R. Lundin, H. Andersson, J. Gimholt, M. Holmström, O. Norberg, M. Yamauchi, K. Asamura, A. J. Coates, D. R. Linder, D. O. Kataria, C. C. Curtis, K. C. Hsieh, B. R. Sandel, A. Fedorov, A. Grigoriev, E. Budnik, M. Grande, M. Carter, D. H. Reading, H. Koskinen, E. Kallio, P. Riihela, T. Säles, J. Kozyra, N. Krupp, S. Livi, J. Woch, J. Luhmann, S. McKenna-Lawlor, S. Orsini, R. Cerulli-Irelli, M. Maggi, A. Morbidini, A. Mura, A. Milillo, E. Roelof, D. Williams, J.-A. Sauvaud, J.-J. Thocaven, T. Moreau, D. Winningham, R. Frahm, J. Scherrer, J. Sharber, P. Wurz, and P. Bochsler, 2004. ASPERA-3: Analyser of space plasmas and energetic ions for Mars Express, in *Mars Express: The scientific payload*, vol. SP-1240, edited by A. Wilson, pp. 121–139, ESA Special Publication.
- Brinkfeldt, K., H. Gunell, P. Brandt, S. Barabash, R. A. Frahm, J. D. Winningham, E. Kallio, M. Holmström, Y. Futaana, A. Ekenbäck, R. Lundin, H. Andersson, M. Yamauchi, A. Grigoriev, J. R. Sharber, J. Scherrer, A. J. Coates, D. R. Linder, D. O. Kataria, H. Koskinen, T. Säles, P. Riihela, W. Schmidt, J. Kozyra, J. Luhmann, E. Roelof, D. Williams, S. Livi, C. C. Curtis, K. C. Hsieh, B. R. Sandel, M. Grande, M. Carter, J.-A. Sauvaud, A. Fedorov, J.-J. Thocaven, S. McKenna-Lawler, S. Orsini, R. Cerulli-Irelli, M. Maggi, P. Wurz, P. Bochsler, N. Krupp, J. Woch, M. Fraenz, K. Asamura, and C. Dierker, 2006. First ena observations at Mars: Solar-wind ENAs on the nightside, *Icarus*, 182 (2), 439–447.
- Crider, D. H., M. H. Acuña, J. E. P. Connerney, D. Vignes, N. F. Ness, A. M.

- Krymskii, T. K. Breus, H. Rème, C. Mazelle, D. L. Mitchell, R. P. Lin, P. A. Cloutier, and D. Winterhalter, 2002. Observations of the latitude dependence of the location of the martian magnetic pileup boundary, *Geophys. Res. Lett.*, *29*(8), 1170, doi:10.1029/2001GL013860.
- Crider, D. H., D. Vignes, A. M. Krymskii, T. K. Breus, N. F. Ness, D. L. Mitchell, J. A. Slavin, and M. H. Acuña, 2003. A proxy for determining solar wind dynamic pressure at Mars using Mars Global Surveyor data, *J. Geophys. Res.*, *108*(A12), 1461, doi:10.1029/2003JA009875.
- Espley, J. R., P. A. Cloutier, D. A. Brain, D. H. Crider, and M. H. Acuña, 2004. Observations of low-frequency magnetic oscillations in the Martian magnetosheath, magnetic pileup region and tail, *J. Geophys. Res.*, *109*, A07213, doi:10.1029/2003JA010193.
- Feldman, W. C., R. C. Anderson, S. J. Bame, J. T. Gosling, R. D. Zwickl, and E. J. Smith, 1983. Electron velocity distributions near the interplanetary shocks, *J. Geophys. Res.*, *88*, 9949–9958.
- Fox, J. L., and A. Dalgarno, 1979. Ionization, luminosity, and heating of the upper atmosphere of mars, *J. Geophys. Res.*, *84*(A12), 7315–7333.
- Futaana, Y., S. Barabash, A. Grigoriev, M. Holmström, E. Kallio, P. C:son Brandt, H. Gunell, K. Brinkfeld, R. Lundin, H. Andersson, M. Yamauchi, S. McKenna-Lawlor, J. D. Winningham, R. A. Frahm, J. R. Sharber, J. Scherrer, A. J. Coates, D. R. Linder, D. O. Kataria, T. Säles, P. Riihela, W. Schmidt, H. Koskinen, J. Kozyra, J. Luhmann, E. Roelof, D. Williams, S. Livi, C. C. Curtis, K. C. Hsieh, B. R. Sandel, M. Grande, M. Carter, J.-A. Sauvaud, A. Fedorov, J.-J. Thocaven, S. Orsini, R. Cerulli-Irelli, M. Maggi, P. Wurz, P. Bochsler, A. Galli, N. Krupp, J. Woch, M. Fraenz, K. Asamura, and C. Dierker, 2006a. First ENA observations at Mars: ENA emissions from the Martian upper atmosphere, *Icarus*, *182* (2), 424–430.

Futaana, Y., S. Barabash, A. Grigoriev, M. Holmström, E. Kallio, P. C:son Brandt, H. Gunell, K. Brinkfeld, R. Lundin, H. Andersson, M. Yamauchi, S. McKenna-Lawlor, J. D. Winningham, R. A. Frahm, J. R. Sharber, J. Scherrer, A. J. Coates, D. R. Linder, D. O. Kataria, T. Säles, P. Riihela, W. Schmidt, H. Koskinen, J. Kozyra, J. Luhmann, E. Roelof, D. Williams, S. Livi, C. C. Curtis, K. C. Hsieh, B. R. Sandel, M. Grande, M. Carter, J.-A. Sauvaud, A. Fedorov, J.-J. Thocaven, S. Orsini, R. Cerulli-Irelli, M. Maggi, P. Wurz, P. Bochsler, N. Krupp, J. Woch, M. Fraenz, K. Asamura, and C. Dierker, 2006b. First ENA observations at Mars: Subsolar ENA jet, *Icarus*, *182* (2), 413–423.

Gunell, H., K. Brinkfeldt, M. Holmström, P. Brandt, S. Barabash, E. Kallio, A. Ekenbäck, Y. Futaana, R. Lundin, H. Andersson, M. Yamauchi, A. Grigoriev, J. D. Winningham, R. A. Frahm, J. R. Sharber, J. Scherrer, A. J. Coates, D. R. Linder, D. O. Kataria, T. Säles, P. Riihela, W. Schmidt, H. E. J. Koskinen, J. Kozyra, J. Luhmann, E. Roelof, D. Williams, S. Livi, C. C. Curtis, K. C. Hsieh, B. R. Sandel, M. Grande, M. Carter, J.-A. Sauvaud, A. Fedorov, J.-J. Thocaven, S. McKenna-Lawlor, S. Orsini, R. Cerulli-Irelli, M. Maggi, P. Wurz, P. Bochsler, N. Krupp, J. Woch, M. Fraenz, K. Asamura, and C. Dierker, 2006. First ENA observations at Mars: Charge exchange ENAs produced in the magnetosheath, *Icarus*, *182* (2), 439–447.

Holmström, M., S. Barabash, and E. Kallio, 2002. Energetic neutral atoms at Mars: 1. Imaging of solar wind protons, *J. Geophys. Res.*, *107*(A10), 1277, doi:10.1029/2001JA000325.

Kallio, E., and S. Barabash, 2001. Atmospheric effects of precipitation energetic hydrogen atoms on the Martian atmosphere, *J. Geophys. Res.*, *106*(A1), 165–177.

- Kallio, E., J. G. Luhmann, and S. Barabash, 1997. Charge exchange near Mars: The solar wind absorption and energetic neutral atom production, *J. Geophys. Res.*, *102*(A10), 22,183–22,197.
- Kallio, E., S. Barabash, K. Brinkfeldt, H. Gunell, M. Holmström, Y. Futaana, W. Schmidt, T. Säles, H. Koskinen, P. Riihelä, R. Lundin, H. Andersson, M. Yamauchi, A. Grigoriev, J. D. Winningham, R. A. Frahm, J. R. Sharber, J. Scherrer, A. J. Coates, D. R. Linder, D. O. Kataria, J. Kozyra, J. G. Luhmann, E. Roerof, D. Williams, S. Livi, P. C. Brandt, C. C. Curtis, K. C. Hsieh, B. R. Sandel, M. Grande, M. Carter, J. A. Sauvaud, A. Fedorov, J. J. Thocaven, S. McKenna-Lawler, S. Orsini, R. Cerulli-Irelli, M. Maggi, P. Wurz, P. Bochsler, N. Krupp, J. Woch, M. Fränz, K. Asamura, and C. Dierker, 2006. Energetic neutral atoms (ENA) at Mars: Properties of the hydrogen atoms produced upstream of the Martian bow shock and implications for ENA sounding technique around non-magnetized planets, *Icarus*, *182*(2), 448–463.
- Lichtenegger, H., H. Lammer, and W. Stumptner, 2002. Energetic neutral atoms at Mars: 3. Flux and energy distributions of planetary energetic H atoms, *J. Geophys. Res.*, *107*(A10), 1279, doi:10.1029/2001JA000322.
- Lundin, R., S. Barabash, H. Andersson, M. Holmström, A. Grigoriev, M. Yamauchi, J.-A. Sauvaud, A. Fedorov, E. Budnik, J.-J. Thocaven, D. Winningham, R. Frahm, J. Scherrer, J. Sharber, K. Asamura, H. Hayakawa, A. Coates, D. R. Linder, C. Curtis, K. C. Hsieh, B. R. Sandel, M. Grande, M. Carter, D. H. Reading, H. Koskinen, E. Kallio, P. Riihela, W. Schmidt, T. Säles, J. Kozyra, N. Krupp, J. Woch, J. Luhmann, S. McKenna-Lawler, R. Cerulli-Irelli, S. Orsini, M. Maggi, A. Mura, A. Milillo, E. Roelof, D. Williams, S. Livi, P. Brandt, P. Wurz, and P. Bochsler, 2004. Solar wind-induced atmospheric erosion at Mars: First results from ASPERA-3

- on Mars Express, *Science*, *305*, 1933–1936.
- Mitchell, D. G., S. E. Jaskulek, C. E. Schlemm, E. P. Keath, R. E. Thompson, B. E. Tossman, J. D. Boldt, J. R. Hayes, G. B. Andrews, N. Paschalidis, D. C. Hamilton, R. A. Lundgren, E. O. Tums, P. Wilson IV, H. D. Voss, D. Prentice, K. C. Hsieh, C. C. Curtis, and F. R. Powell, 2000. High energy neutral atom (HENA) imager for the IMAGE mission, *Space Sci. Rev.*, *91*(1-2), 67–112.
- Moore, T. E., D. J. Chornay, M. R. Collier, F. A. Herrero, J. Johnson, M. A. Johnson, J. W. Keller, J. F. Laudadio, J. F. Lobell, K. W. Ogilvie, P. Rozmarynowski, S. A. Fuselier, A. G. Ghielmetti, E. Hertzberg, D. C. Hamilton, R. Lundgren, P. Wilson, P. Walpole, T. M. Stephen, B. L. Peko, B. Van Zyl, P. Wurz, J. M. Quinn, and G. R. Wilson, 2000. The low energy neutral atom imager for IMAGE, *Space Sci. Rev.*, *91*(1-2), 155–195.
- Nagy, A. F., D. Winterhalter, K. Sauer, T. E. Cravens, S. Brecht, C. Mazelle, D. Crider, E. Kallio, A. Zakharov, E. Dubinin, M. Verigin, G. Kotova, W. I. Axford, C. Bertucci, and J. G. Trotignon, 2004. The plasma environment of Mars, *Space Sci. Rev.*, *111*, 33–114.
- Peréz-de-Tejada, H., 1987. Plasma flow in the Mars magnetosphere, *J. Geophys. Res.*, *92*, 4713–4718.
- Pollock, C. J., K. Asamura, J. Baldonado, M. M. Balkey, P. Barker, J. L. Burch, E. J. Korpela, J. Cravens, G. Dirks, M.-C. Fok, H. O. Funsten, M. Grande, M. Gruntman, J. Hanley, J.-M. Jahn, M. Jenkins, M. Lampton, M. Marckwordt, D. J. McComas, T. Mukai, G. Penegor, S. Pope, S. Ritzau, M. L. Schattenburg, E. Scime, R. Skoug, W. Spurgeon, T. Stecklein, S. Storms, C. Urdiales, P. Valek, J. T. M. van Beek, S. E. Weidner, M. Wüest, M. K. Young, and C. Zinsmeyer, 2000. Medium energy neutral atom (MENA) imager for the IMAGE mission, *Space Sci. Rev.*, *91*(1-2),

113–154.

Roelof, E. C., D. G. Mitchell, and D. J. Williams, 1985. Energetic neutral atoms ($E \sim 50$ keV) from the ring current: IMP 7/8 and ISEE 1, *J. Geophys. Res.*, *90*, 10,991–11,008.

Sagdeev, R. Z., and A. V. Zakharov, 1989. Brief history of the Phobos mission, *Nature*, *341* (6243), 581–585.

Thomsen, M. F., 1985. Upstream suprathermal ions, in *Collisionless shocks in the heliosphere: Reviews of current research*, edited by B. T. Tsurutani and R. G. Stone, pp. 253–270, American Geophysical Union.

Treumann, R. A., and T. Terasawa, 2001. Electron acceleration in the heliosphere, *Space Sci. Rev.*, *99*, 135–150.

Vaisberg, O. L., 1992. The solar wind interaction with Mars: A review of results from early Soviet missions to Mars, in *Venus and Mars: Atmospheres, Ionospheres, and Solar Wind Interactions*, AGU Geophysical Monograph, vol. 66, edited by J. G. Luhmann, M. Tatralay, and R. O. Pepin, pp. 311–326.

Vignes, D., C. Mazelle, H. Rème, M. H. Acuña, J. E. P. Connerney, R. P. Lin, D. L. Mitchell, P. Cloutier, D. H. Crider, and N. F. Ness, 2000. The solar wind interaction with Mars: locations and shapes of the bow shock and the magnetic pile-up boundary from the observations of the MAG/ER experiment onboard Mars Global Surveyor, *Geophys. Res. Lett.*, *27*(1), 49–52.

Vignes, D., M. H. Acuña, J. E. P. Connerney, D. H. Crider, H. Rème, and C. Mazelle, 2002. Factors controlling the location of the bow shock at Mars, *Geophys. Res. Lett.*, *9*, 1328, doi:10.029/2001GL014513.

Acknowledgments

Y. Futaana has been supported by a Postdoctoral Fellowship for Research Abroad program from the Japan Society for the Promotion of Science and by a JSPS Research Fellowships for Young Scientists. We would like to acknowledge Dr. Mario Acuña at NASA/GSFC and the MGS MAG/ER team for providing the dynamic pressure data at Mars and thank Dr. D. Crider at the Catholic University of America for fruitful discussion concerning the MGS data. The work at SwRI was supported by NASA contract NASW0003. The ASPERA-3 experiment on the European Space Agency (ESA) Mars Express is a joint effort among 15 laboratories in 10 countries, all supported by their national agencies. We thank all these agencies, as well as the various departments and institutes hosting these efforts.

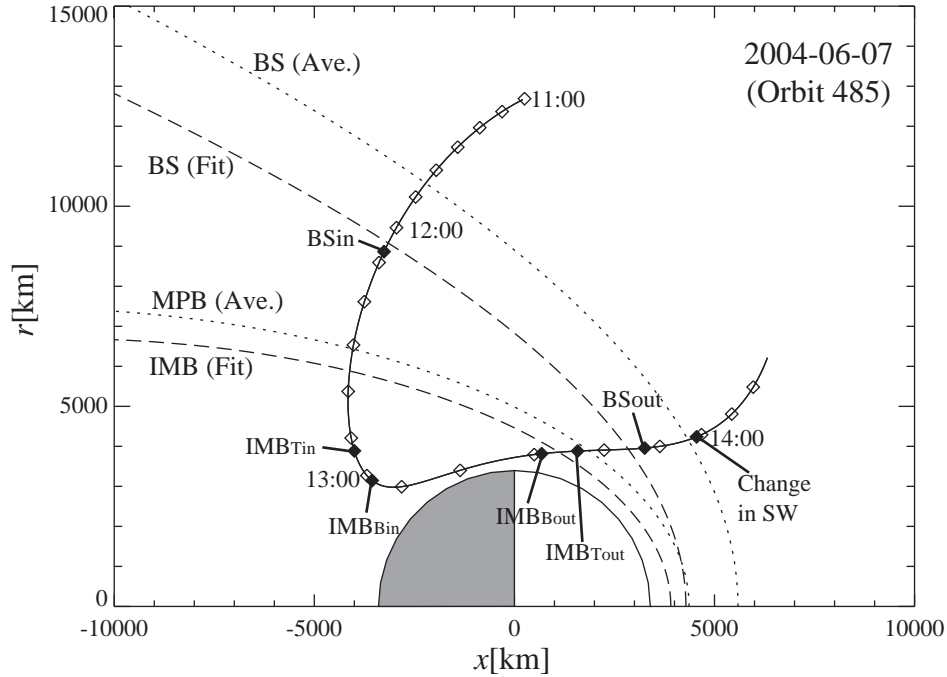


Fig. 1. The orbit of Mars Express on June 7, 2004 (orbit 485) in the cylindrical coordinate system. The periapsis occurred at 13:22:26 UT. The dotted lines are the averaged locations of the bow shock (BS) and the magnetic pileup boundary (MPB) described in *Vignes et al.* (2000). The bow shock and the induced magnetosphere boundary (IMB) crossings are shown by filled symbols. The satellite position when the change in solar wind conditions was observed (13:58:30 UT) is also indicated. The dashed lines are the calculated positions of bow shock and induced magnetosphere boundary assuming the scaling law.

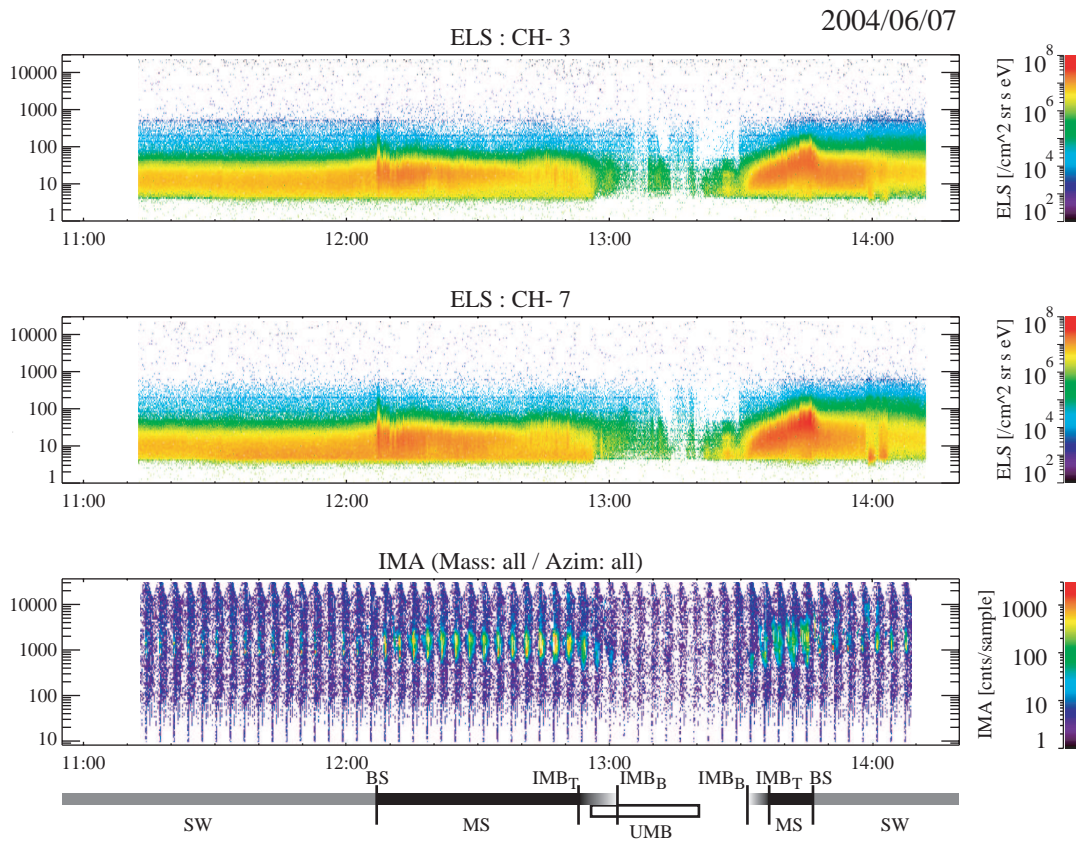


Fig. 2. The electron and ion observations throughout the observation for orbit 485. The first and second panel shows the ELS energy-time spectrogram (Ch-3 and -7), and the third panel shows the IMA energy-time spectrogram summed over all view directions and mass channels. At the bottom, plasma boundaries and domains are denoted, where BS is the bow shock, IMB is the induced magnetosphere boundary, SW is the solar wind, MS is the magnetosheath, and UMB is the umbra.

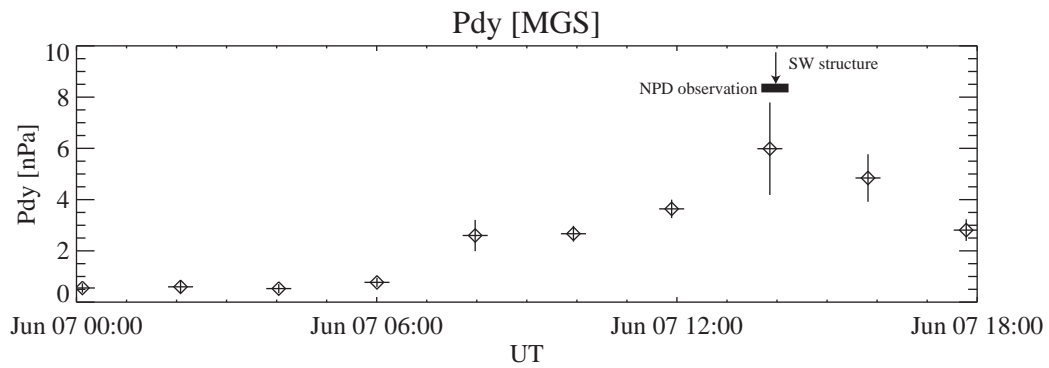


Fig. 3. Solar wind dynamic pressure estimated by MGS observations [*Crider et al.* (2003)]. The estimates were performed by fitting the magnetic field data obtained in the dayside northern hemisphere (~ 30 min). The NPD observation time (13:42-14:13UT) is shown by a filled rectangle, and the arrival time of the solar wind structure detected by Mars Express ($\sim 13:58:30$ UT) is shown by the arrow.

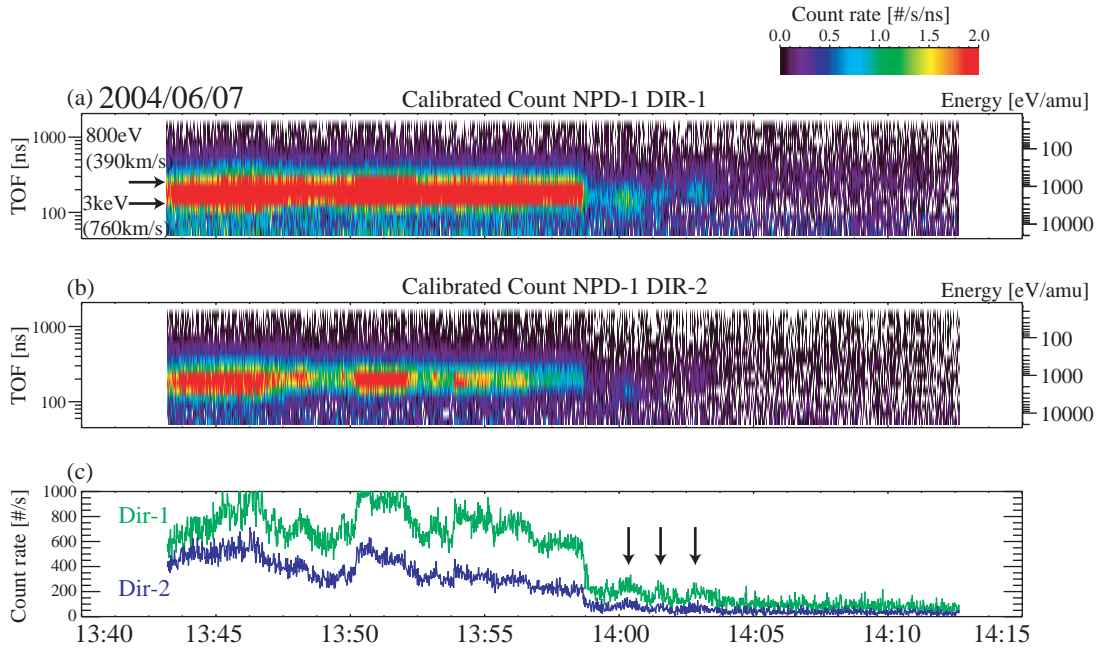


Fig. 4. Time of flight spectrum of NPD-1 for (a) DIR-1 and (b) DIR-2. The energy corresponding to the time of flight (assuming mass=1 amu) is shown on the right axis. The intense signal with energies 0.8-3.0 keV is the subsolar-ENA flux. (c) The count rate of the subsolar ENA flux integrated over the time of flight. Abrupt depletion of ENA fluxes occurred at $\sim 13:58:40$ UT. Following variations in flux are depicted by arrows.

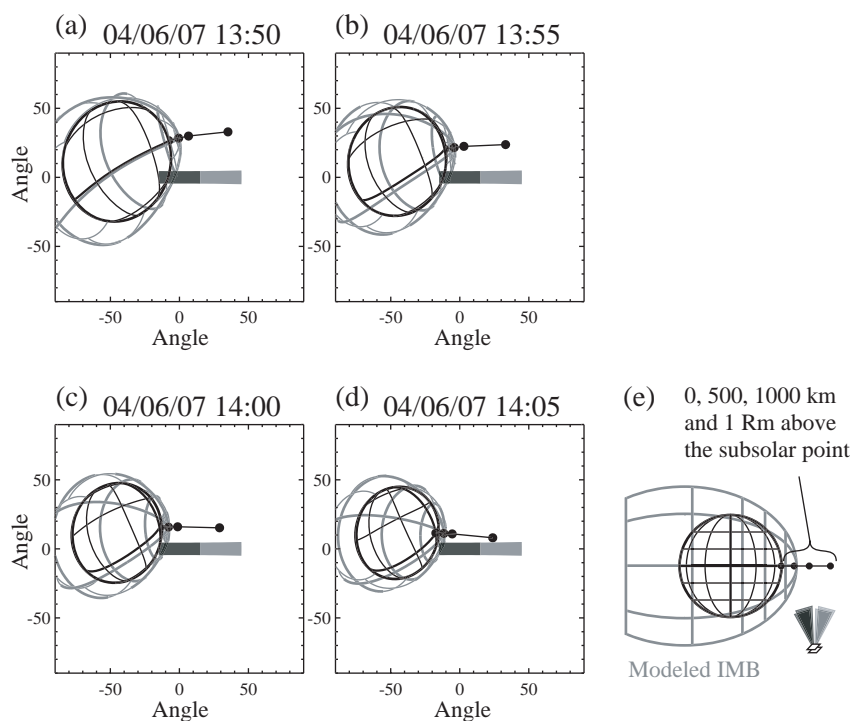


Fig. 5. (a)-(d) Time series of the geometry of Mars with respect to the fields of view of the Dir-1 (dark gray) and Dir-2 (light gray). The cartoon (e) is the legend for the projection of the panels (a)-(d). The projection is determined with respect to the center of Dir-1. The FOVs of the NPD are fixed in this projection. Mars and the fitted IMB (see Figure 1) are shown by the black and the light gray curves. The Mars-sun line is indicated by a black hair line and the point at 0, 500, 1000, and 3397 km above the subsolar point are identified by black symbols.

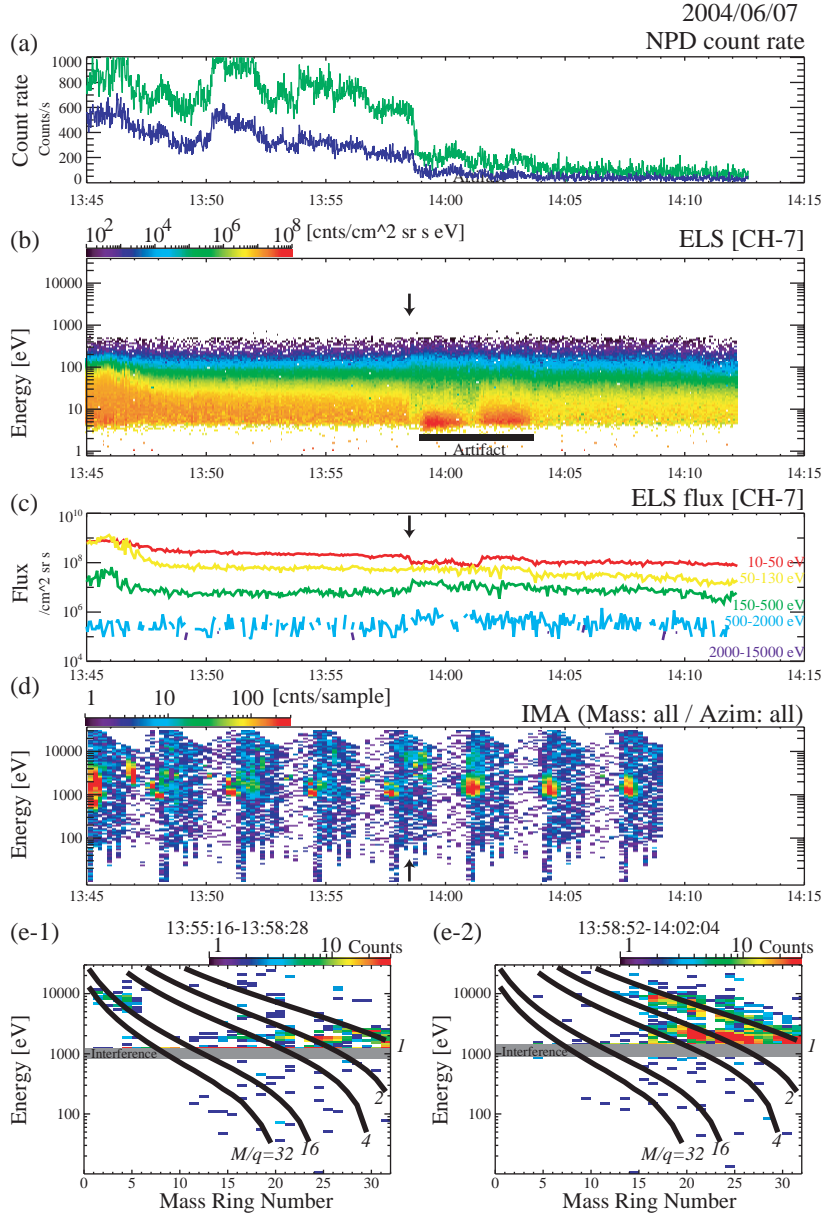


Fig. 6. The simultaneous observations from IMA and ELS. The top panel (a) is the integrated ENA flux (identical to Fig. 4(c)). The panel (b) shows the energy-time spectrogram observed by ELS. The panel (c) shows the time series of counts with the energy range 10-50, 50-130, 150.0-500, 500-2000 and 2000-15000 eV from ELS. The panel (d) shows the IMA energy-time spectrogram between 13:45 and 14:15 (Operation ended at 14:09 UT). The bottom panels (e-1) and (e-2) display the energy-mass spectra as measured by IMA. The thick lines correspond to the mass per charge profiles of the observed ions for $M/q=1, 2, 4, 16$ and 32 .

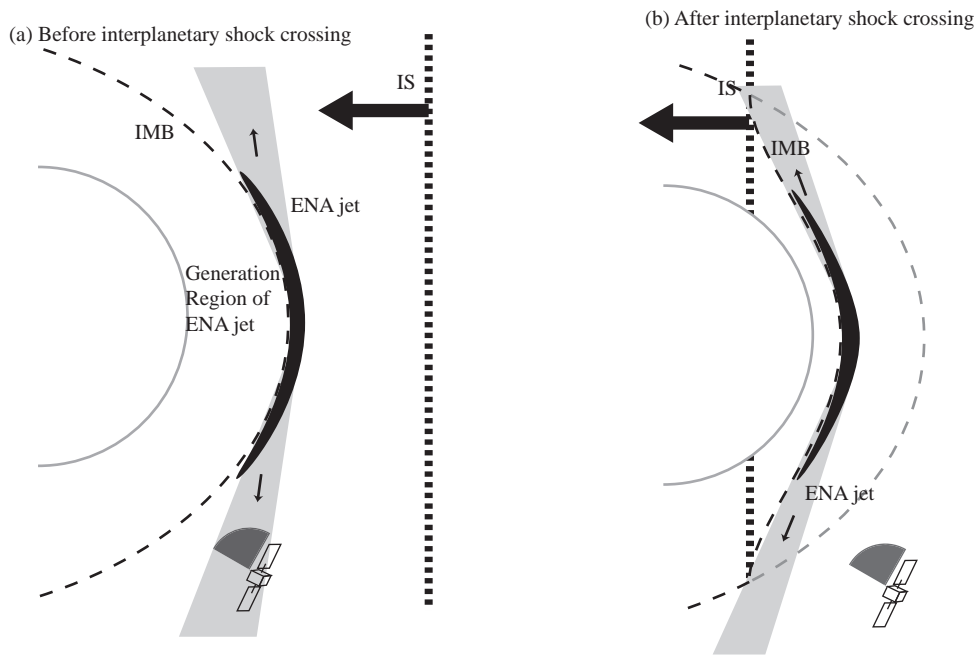


Fig. 7. Illustration of the interpretation (see text for details): (a) before and (b) after the shock crossing of the planetary ENA jet source. The source region of the subsolar ENA jet, which is very close to the IMB, was pushed toward the planet due to the high dynamic pressure of the interplanetary shock. The satellite went out of the subsolar ENA jet very quickly due to this reconfiguration of the Martian plasma obstacle.

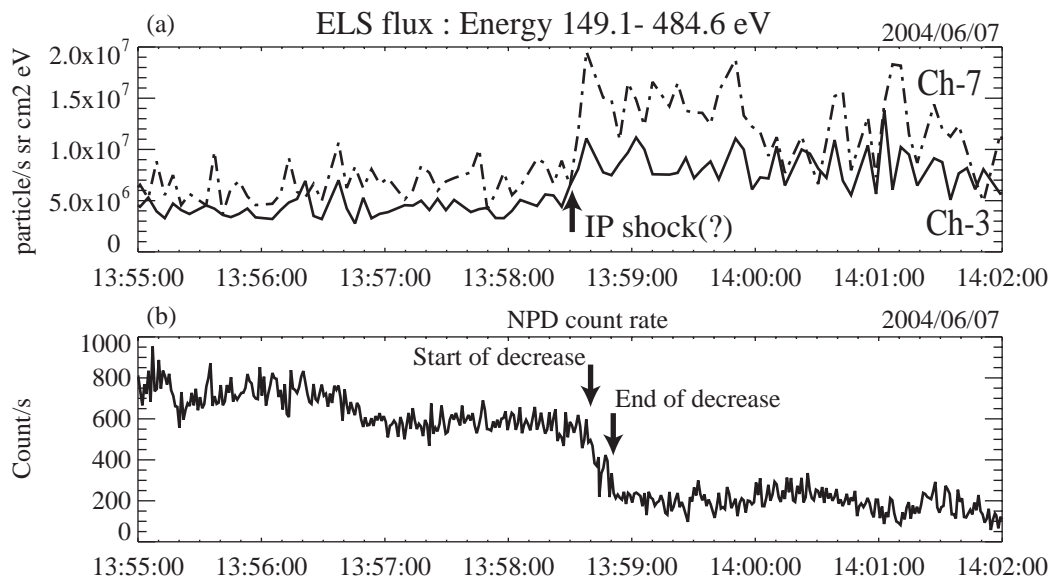


Fig. 8. Electron and ENA flux around the shock crossing (13:55-14:02 UT): (a) The electron flux with energies between 149.1-484.6 eV (identical to the green line in Figure 6(c)). (b) The ENA count rate (identical to the green line in Figure 4(c)).